Genome Biology

RESEARCH

Open Access

MORC proteins regulate transcription factor binding by mediating chromatin compaction in active chromatin regions

Zhenhui Zhong[1†], Yan Xue[1,2†], C. Jake Harris[1,3], Ming Wang[1], Zheng Li[1], Yunqing Ke[1], Mukun Liu[1], Jessica Zhou[1], Yasaman Jami-Alahmadi[4], Suhua Feng[1,5], James A. Wohlschlegel[4] and Steven E. Jacobsen[1,6*]

†Zhenhui Zhong and Yan Xue contributed equally to this work.

*Correspondence: jacobsen@ucla.edu

[1] Department of Molecular, Cell and Developmental Biology, University of California, Los Angeles, CA 90095, USA
[2] Shandong Laboratory of Advanced Agricultural Sciences at Weifang, Peking University Institute of Advanced Agricultural Sciences, Weifang 261000, Shandong, China
[3] Department of Plant Sciences, University of Cambridge, Cambridge CB2 3EA, UK
[4] Department of Biological Chemistry, University of California, Los Angeles, CA 90095, USA
[5] Eli & Edythe Broad Center of Regenerative Medicine & Stem Cell Research, University of California, Los Angeles, CA 90095, USA
[6] Howard Hughes Medical Institute, University of California, Los Angeles, CA 90095, USA

Abstract

Background: The microrchidia (MORC) proteins are a family of evolutionarily conserved GHKL-type ATPases involved in chromatin compaction and gene silencing. Arabidopsis MORC proteins act in the RNA-directed DNA methylation (RdDM) pathway, where they act as molecular tethers to ensure the efficient establishment of RdDM and de novo gene silencing. However, MORC proteins also have RdDM-independent functions although their underlying mechanisms are unknown.

Results: In this study, we examine MORC binding regions where RdDM does not occur in order to shed light on the RdDM-independent functions of MORC proteins. We find that MORC proteins compact chromatin and reduce DNA accessibility to transcription factors, thereby repressing gene expression. We also find that MORC-mediated repression of gene expression is particularly important under conditions of stress. MORC-regulated transcription factors can in some cases regulate their own transcription, resulting in feedback loops.

Conclusions: Our findings provide insights into the molecular mechanisms of MORC-mediated chromatin compaction and transcription regulation.

Keywords: Microrchidia, MORC, Chromatin compaction, TF binding, Transcription regulation

Background

The MORC proteins are a family of highly conserved GHKL-type ATPases involved in gene silencing and chromatin compaction [1]. In *Caenorhabditis elegans*, MORC-1 can compact DNA through topological entrapment [2], while in humans, MORC2 is recruited by the human silencing hub (HUSH) complex for H3K9me3 deposition, chromatin compaction, and gene silencing [3]. In mice, MORC1 is involved in germline transposon silencing [4], and MORC3 is essential for transposon silencing in embryonic stem cells [5].

The Arabidopsis genome encodes six MORC proteins: MORC1, 2, 4, 5, 6, and 7 (MORC3 being a pseudogene) [6]. These six proteins are functionally redundant and colocalize with sites of RNA-directed DNA methylation (RdDM) genome-wide [7], where they are critical for establishing efficient RdDM and de novo gene silencing [7]. MORC7, when tethered to DNA using an artificial zinc finger, can target RdDM to ectopic sites. MORC7 is also required for the silencing of newly integrated *FWA* transgenes [7]. MORC proteins also act downstream of DNA methylation to suppress gene expression and are also involved in plant immunity — protecting plants against potential pathogens by interacting with plant resistance (R) proteins [8, 9]. However, the molecular mechanisms underlying these RdDM-independent functions remain unknown. We previously observed MORC binding sites where RdDM does not occur (MORC-unique sites) [7], and by studying these sites, we aim to shed light on the mechanisms underlying the RdDM-independent functions of MORC proteins.

TOPLESS (TPL) and LEUNIG (LUG) are both Grocho (Gro)/TLE-type transcriptional co-repressors in plants. They are characterized by a conserved glutamine-rich C-terminal domain and an N-terminal WD-repeat domain [10]. The glutamine-rich domain participates in protein oligomerization, and the WD-repeat domain interacts with downstream transcriptional regulators [10]. The functional counterpart of the Gro/TLE family of proteins in yeast, Tup1, was originally identified as a co-repressor that occupied the binding sites of transcriptional activators [11, 12]. However, evidence now shows that Tup1 can switch from a co-repressor to a co-activator in response to stress, and is required for the activation of certain genes related to the stress response [11, 12].

Here, we use MORC-unique sites to study the RdDM-independent functions of MORC proteins. We show that MORC proteins compact chromatin and reduce DNA accessibility to TFs, thereby repressing the transcription of stress-responsive genes.

Results

MORC proteins bind to active chromatin regions devoid of RdDM

We previously reported that approximately 80% of MORC7 binding regions overlap with sites of RdDM [7]. MORC7 is recruited to these sites by the RdDM machinery, where it then facilitates the efficiency of the RdDM pathway. However, the remaining 20% of MORC7 binding sites are devoid of RdDM, as evidenced by a lack of Pol V occupancy [7]. The mechanisms underlying the function of MORC7 within these RdDM-depleted regions remain unknown.

Mouse MORC3 recognizes and localizes to regions of H3K4me3-marked chromatin through its CW domain [13]; however, Arabidopsis MORCs do not contain CW domains. To determine whether Arabidopsis MORCs co-localize with specific chromatin features, we used the ChromHMM method to investigate correlations between MORC7 and several well-characterized chromatin features (H3K9ac, H3K27ac, H4K16ac, H3K4me1, H3K4me3, H3K36me2, H3K36me3, H3K9me2, H3K27me3, Pol II, and Pol V). We analyzed chromatin states using a similar method as previously reported [14] but also included Pol V ChIP-seq data. We found 13 different chromatin states (Additional file 1: Fig. S1). MORC7 showed a strong correlation with Pol V (a known indicator of RdDM sites), which was consistent with our previous findings (State 11, Additional file 1: Fig. S1). Chromatin state 12 included sites enriched with MORC7 but

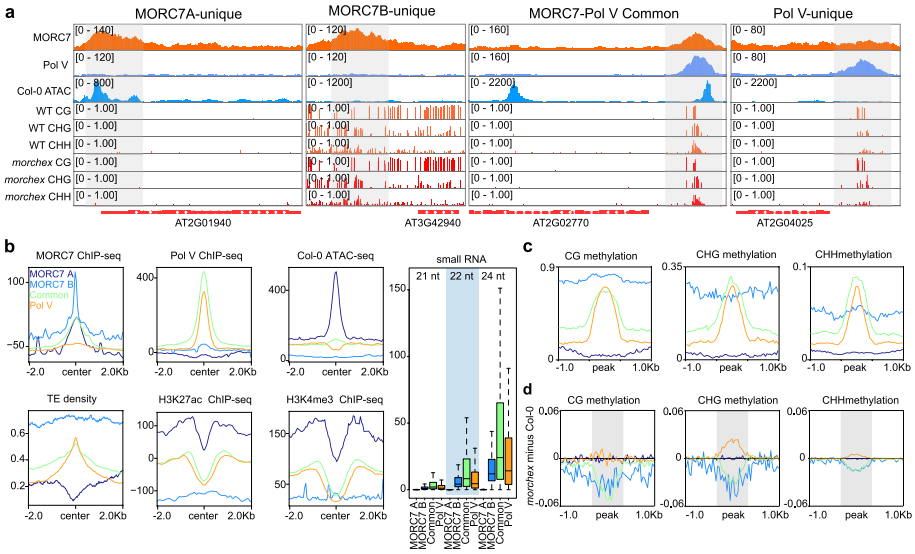

Fig. 1 MORC7 binds to regions devoid of RdDM. **a** Screenshots of ChIP-seq data for MORC7A-unique, MORC7B-unique, MORC7-Pol V Common, and Pol V-unique regions. **b** Metaplots of ChIP-seq data for MORC7, Pol V, H3K27ac, H3K4me3, ATAC-seq, transposable element (TE), and small RNA density over regions of MORC7A-unique, MORC7B-unique, MORC7-Pol V Common, and Pol V-unique. **c** Metaplot showing methylation levels of CG, CHG, and CHH, over regions of MORC7A-unique, MORC7B-B unique, MORC7-Pol V Common, and Pol V-unique. **d** Metaplot showing methylation levels of CG, CHG, and CHH methylation changes (*morchex* minus WT) over regions of MORC7A-unique, MORC7B-unique, MORC7-Pol V Common, and Pol V-unique

depleted of Pol V — indicative of MORC7-unique regions. We did not observe enrichment of histone marks in these MORC7-unique regions (Additional file 1: Fig. S1).

Within these MORC7-unique regions, we identified two subgroups: MORC7A and MORC7B. The ChIP-seq data for MORC7, Pol V, ATAC-seq, transposable element (TE), and small RNA density indicated that MORC7A was within a region of high chromatin accessibility and low TE density (Fig. 1a, b, Additional file 1: Fig. S2). Consistent with the ChromHMM analysis, MORC7A displayed low levels of histone occupancy and histone modification, although its flanking regions were enriched for active histone modifications. This suggests that MORC7A is located within an active chromatin compartment between genes (Fig. 1b).

MORC7B contained a high density of TE with no apparent active histone marks, reflective of its heterochromatic localization (Fig. 1a, b). We found that MORC7A regions had low levels of DNA methylation, while MORC7B regions had high levels of methylation (Fig. 1c, d). These results suggest that MORC7 binds to active and deep heterochromatic regions of DNA, where RdDM does not occur, suggesting that it regulates gene expression at these sites through RdDM-independent mechanisms.

MORC7 preferentially binds to the promoters of TFs

The genomic distribution enrichment data showed enrichment of MORC7A peaks over promoters (Fig. 2a), but no enrichment of MORC7B peaks — consistent with their deep heterochromatic localization. The functional annotation of the genes proximal to MORC7A suggested that they were enriched in TF encoding genes (Table 1). The Arabidopsis genome encodes approximately 1491 TF genes (5.5% of the genome) [15]. Of

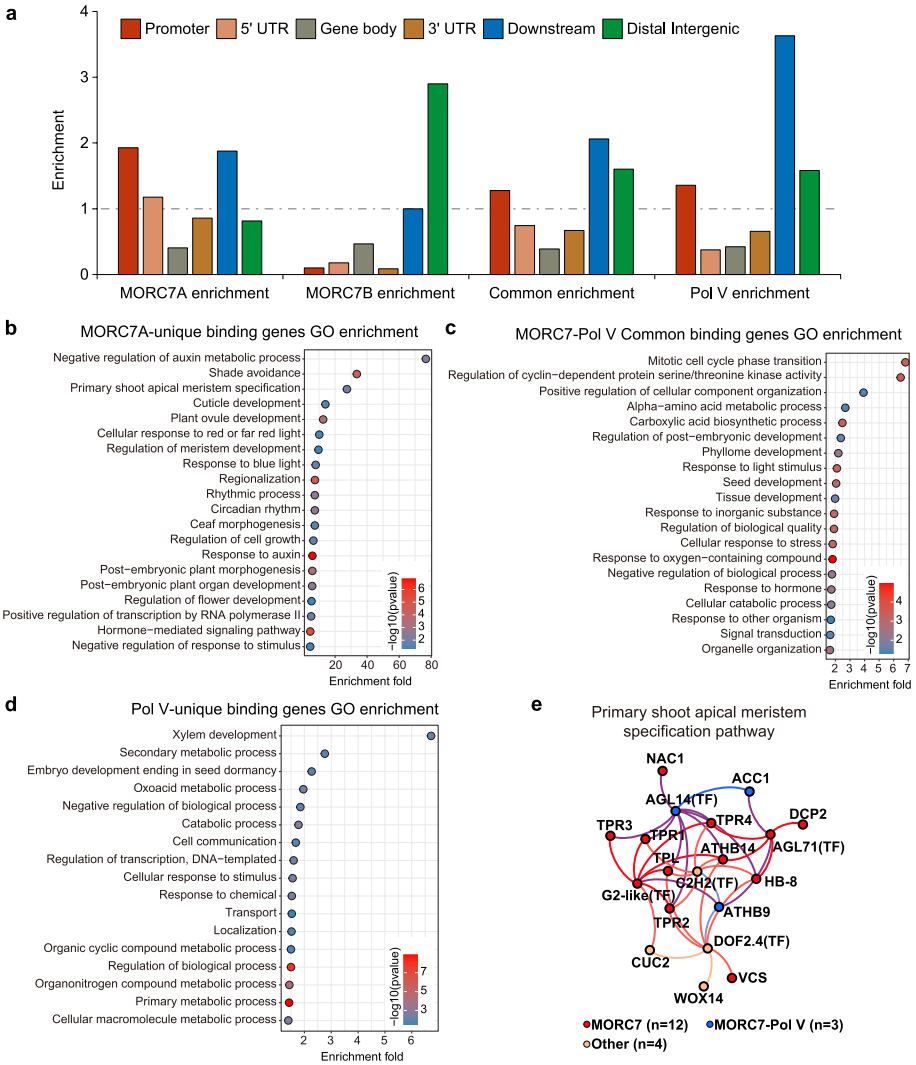

Fig. 2 MORC7-unique regions preferentially localize to the promoter regions of TFs. **a** Genomic distribution enrichment data for MORC7A-unique, MORC7B-unique, MORC7-Pol V Common, and Pol V-unique regions. Gene ontology enrichment data for the proximal genes of MORC7A (**b**), MORC7-Pol V Common (**c**), and Pol V-unique regions (**d**). **e** MORC7 and Pol V binding on promoters of genes in the primary shoot apical meristem specification pathway

Table 1 Number of TFs among the proximal genes of MORC7A-unique, MORC7B-unique, MORC7-Pol V Common, and Pol V-unique regions. *P*-values are estimated by hypergeometric test

Peak	TF	Non-TF	Total	Percentage	*p*-value
MORC7A	99	326	425	23.29%	3.12E − 36
MORC7B	6	27	33	18.18%	0.002
MORC7-Common	114	1475	1589	7.17%	0.001
Pol V	98	1080	1178	8.32%	1.60E − 05
Whole genome	1491	25,681	27,172	5.49%	NA

the genes proximal to MORC7A, 23% were TFs (p-value = 3.12E − 36); these included PHYTOCHROME INTERACTING FACTOR (PIF), ethylene and auxin-responsive transcriptional factors, and Myb transcriptional factors (Additional file 2: Table S1).

This enrichment was more significant than enrichment for MORC7-Pol V common (p-value = 0.001) and Pol V-unique (p-value = 1.6E − 5).

Gene Ontology (GO) term analysis of genes proximal to MORC7A showed an enrichment of negative regulation of auxin metabolic process (~80-fold), shade avoidance (~30 fold), and the primary shoot apical meristem specification pathway (~30-fold) (Fig. 2b, c, d). The primary shoot apical meristem specification pathway (GO0010072) is responsible for the growth of all post-embryonic, above-ground plant structures [16]. In Arabidopsis, this pathway includes several topless-related genes [16]. Interestingly, we found that MORC7 specifically bound to 12 of the 19 genes in this pathway (Fig. 2e, Additional file 1: Fig. S3), and co-localized with Pol V at an additional three. We show examples of MORC7 enrichment over the promoter regions for the four TOPLESS genes in Additional file 1: Fig. S3.

MORC7 closely co-localizes with some TFs

To investigate the protein interaction network of MORC7 with chromatin, we re-analyzed previously published crosslinked IP-MS data of MORC7 [7]. We identified 494 proteins (FDR < 0.05, FC > 2) that interacted with MORC7 (Fig. 3a), and found that many of these were involved in either chromatin-related pathways or development (Fig. 3b). We also identified 68 TFs from the MORC7 interacting proteins (68/494, p = 7.89E − 12)

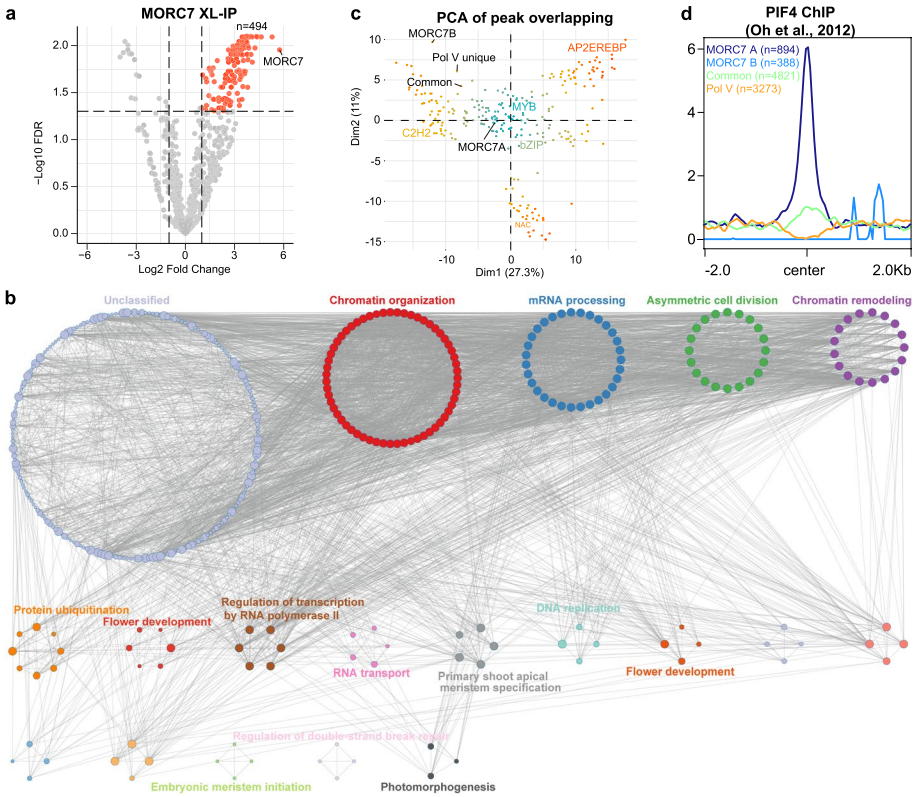

Fig. 3 MORC7 associates with some TFs. **a** Volcano plot showing proteins that have significant interactions with MORC7, as detected by crosslinked IP-MS. **b** Protein–protein interaction networks of MORC7. **c** A graph showing the degree of overlap between the DAP-seq peaks of approximately 200 TFs with MORC7A-unique, MORC1B-unique, MORC7-Pol V Common, and Pol V unique regions. **d** Metaplot of PIF4 ChIP-seq data [18] over MORC7A-unique, MORC7B-unique, MORC7-Pol V Common, and Pol V unique regions

(Additional file 3: Table S2). To further test whether MORC7 co-localizes with TFs, we obtained binding site information for 200 TFs from the DNA Affinity Purification and sequencing (DAP-seq) database [17], and performed pairwise peak overlap analysis with MORC7 peaks. We found that MORC7A showed stronger co-localization with TFs compared to MORC7B, MORC7-Pol V common, and Pol V-unique regions, and also showed strong co-localization with some TF binding sites but not others (Fig. 3c). For the TFs characterized with DAP-seq, we found 23 TFs pull downed by MORC7 crosslinked IP-MS data (Additional file 3: Table S2). This indicates that MORC7A peaks are associated with TF binding sites. We also re-analyzed three transcription factors, PIF4 [18], ARF6 [19], and TPR1 [20], in particular, because published ChIP-seq data was available. Metaplot analysis with ChIP-seq data indicated that MORC7A-unique, MORC7B-unique, MORC7-Pol V Common, and Pol V-unique regions showed the strongest co-localization with MORC7A, but the random promoter controls didn't show obvious enrichment (Fig. 3d, Additional file 1: Fig. S4).

MORC7 influences TF binding through chromatin compaction

To understand how MORC7 affects chromatin conformation, we performed an Assay for Transposase-Accessible Chromatin with high-throughput sequencing (ATAC-seq) in *morc4 morc7*, *morc6*, and *morc hextuple* (*morchex*, in which all functional MORCs are knocked out) mutants [6]. We plotted ATAC-seq data across the four groups and found that MORC7A, MORC7B, and MORC7-Pol V common showed greater chromatin accessibility changes in the mutants, particularly over the MORC7A regions (Fig. 4a, b). This phenotype is consistently observed in *morc4 morc7*, *morc6*, and *morche*x — with *morchex* showing the most pronounced phenotype (Fig. 4a, Additional file 1: Fig. S5). Interestingly, for Pol V-unique sites, DNA compaction was not reduced, but actually became slightly increased (Fig. 4a). Consistently, we also observed an increase in DNA methylation for Pol V-unique sites in the mutants (Fig. 1d). This suggests that Pol V may be redistributed from the MORC7-Pol V common sites to Pol V-unique sites in the absence of MORC proteins. This is consistent with our previous findings that suggested MORC proteins function as molecular tethers to facilitate the recruitment of RdDM components [7].

To examine whether MORC-mediated DNA compaction affects TFs, we analyzed the ATAC-seq data for TF footprints. When a TF binds to DNA, it inhibits the integration of DNA by Tn5 transposes, causing the binding motif to exhibit lower DNA accessibility, and the flanking regions to exhibit higher DNA accessibility [21]. The footprints of 572 TFs downloaded from JASPAR were analyzed in the *morc4 morc7*, *morc6*, and *morchex* mutants [22]. Many TFs showed substantially stronger apparent binding within the MORC7A regions in the mutants. There were some increases in binding within the MORC7B regions (although to a lesser degree than in MORC7A regions) (Fig. 4c, d), while TF binding over RdDM sites was largely unaffected (Fig. 4e, f). The metaplot of ATAC-seq signals over the TF binding sites for the MORC7A regions confirmed that these TFs have stronger apparent binding in *morc4 morc7*, *morc6*, and *morche*x mutants — with *morchex* showing the strongest binding changes, and the random control regions showing no differences (Fig. 4g–i).

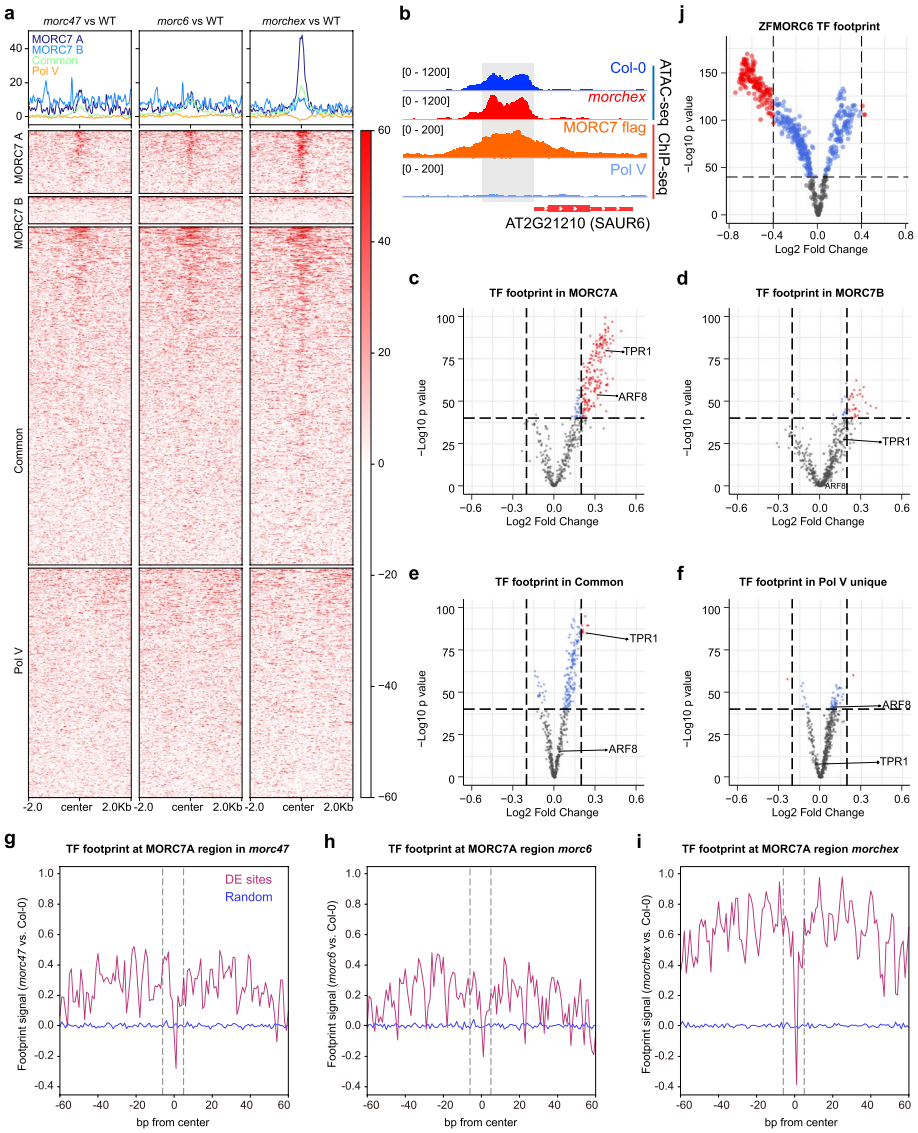

Fig. 4 MORC proteins influence TF binding through chromatin compaction. **a** Metaplot and heatmap showing chromatin accessibility changes in MORC7A-unique, MORC7B-unique, MORC7-Pol V Common, and Pol V-unique regions profiled by ATAC-seq. **b** A representative screenshot showing higher chromatin accessibility at the promoter of SAUR6 in the *morchex* mutant. **c** Volcano plot showing changes in TF footprints in MORC7A regions, comparing *morchex* and wild type. **d** Volcano plot showing changes in TF footprints in MORC7B regions, comparing *morchex* and wild type. **e** Volcano plot showing changes in TF footprints in MORC7-Pol V Common regions, comparing *morchex* and wild type. **f** Volcano plot showing changes in TF footprints at Pol V-unique regions, comparing *morchex* and wild type. **g** Metaplot showing TF footprint changes for MORC7A-unique regions in the *morc4morc7* mutant. **h** Metaplot showing TF footprint changes for MORC7A-unique regions in the *morc6* mutant. **i** Metaplot showing TF footprint changes for MORC7A-unique regions in the *morchex* mutant. **j** Volcano plot showing TF changes for ZF off-target sites, comparing ZF-MORC6 and *fwa-4* plants. *P* values were calculated by the two-sided Student's *t*-test

We previously showed that targeting either MORC7 or MORC6 ectopically in the *fwa-4* epiallele background using ZF108 can trigger the silencing of *FWA* [7, 23]. In addition to the *FWA* locus, ZF108 can also bind thousands of off-target sites [23]. These off-target sites are preferentially localized to promoter regions and therefore

provide an excellent opportunity to test whether the presence of MORC proteins can affect TF binding. We compared TF footprints between ZF-MORC6 and *fwa-4* and found a substantial decrease for many of the TF footprints in ZF-MORC6 plants (Fig. 4j). We further divided ZF off-target sites into sites that gain of DNA methylation ($n = 2186$) or non-gain of DNA methylation ($n = 8580$), and observed a substantial decrease of the TF footprints over both groups of sites in ZF-MORC6 plants (Additional file 1: Fig. S6). This supports the hypothesis that MORC proteins affect TF binding. Together, these results suggest that MORCs inhibit TF binding by altering chromatin accessibility.

MORC influences gene expression downstream of the TFs

To understand whether MORC proteins regulate gene expression, we performed RNA-seq with the *morchex* mutant. As MORC7A co-localizes strongly with PIF4 (Fig. 3d) — a central regulator in temperature signaling [24] — we applied heat treatment to the *morchex* mutant. We first compared the expression of genes proximal to MORC7A peaks in wild type (WT) and *morchex* mutant without treatment. This showed that the genes proximal to MORC7A were slightly ($p = 0.002$) up-regulated in the *morchex* mutant without treatment (Fig. 5a), including the TFs SEP3, PIF4, ARF6/8, TPR1, LUG, and SEU (Fig. 5b). After heat treatment, *morchex* displayed a stronger response compared to the WT, with significantly more upregulated genes (Fig. 5c, d). Genes proximal to MORC7A were enriched in shoot apical meristem specification pathways, and consistently, we observed stronger upregulation of these genes in *morchex* after heat treatment (Additional file 1: Fig. S7).

To confirm that MORC proteins affect TF binding, and to understand how they affect downstream gene expression, we selected two TFs, TOPLESS (TPL) and LEUNIG (LUG), for ChIP-seq analysis, because they were present in the MORC7 IP-MS data [7]. We expressed TPL and LUG fused with a 3XFLAG-tag in both WT and *morchex*. Consistent with the TF footprint analysis, both TPL and LUG displayed stronger binding at MORC7A regions, while only a slight increase in binding was noted for the MORC7-Pol V co-binding sites in *morchex* (Fig. 5e, f) — consistent with an increase in chromatin accessibility in *morchex* (Fig. 5g). To test whether the binding strength of TPL and LUG might be higher in *morchex*, we ranked TPL and LUG binding sites based on the MORC ChIP-seq signals and divided them into three groups: high, middle and low (Fig. 5g). Overall, in the *morchex* mutant, we observed increased TPL and LUG binding, as well as increased chromatin accessibility across the regions with stronger MORC7 signals (Fig. 5g). We found that MORC7A-bound genes were downregulated ($p = 5.7E-13$) in the *lug* mutant, suggesting that LUG may facilitate expression of these genes (Fig. 5a). Using ChIP-seq data together with RNA-seq data in the *lug* mutant, we identified 95 genes that appeared to be directly regulated by LUG (Additional file 4: Table S3). We found that these LUG-regulated genes were upregulated ($p = 0.77$) in *morchex*, particularly after heat treatment ($p = 7.5E-9$, Fig. 5h). Motif enrichment analysis indicated that most overrepresented motifs were largely similar between wild-type and *morchex* mutant (Additional file 1: Fig. S8). However, we identified some peaks by the peak calling method MACS2 in *morchex* mutants that were not called as a peak in wild type. A metaplot of ChIP-seq signal over these regions showed a higher signal for TPL and LUG in *morchex* as compared to wild type (Additional file 1: Fig. S9).

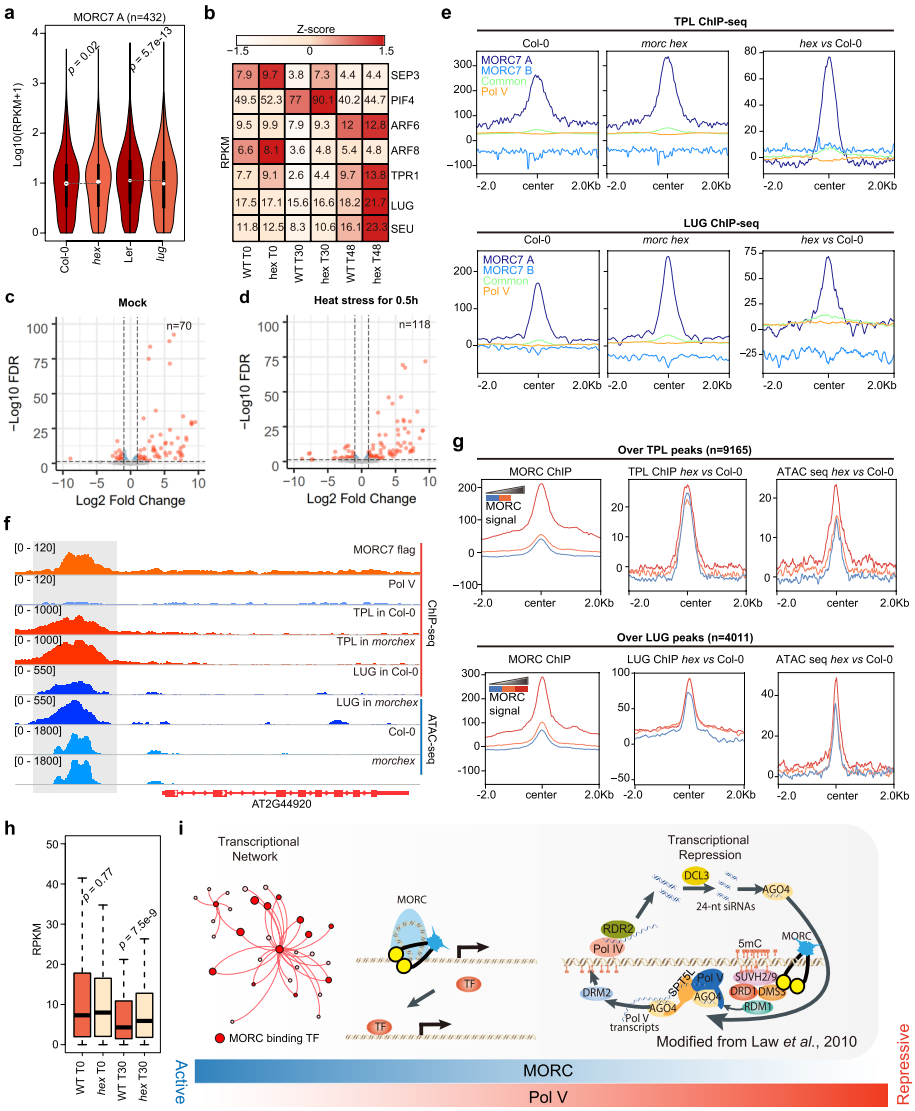

Fig. 5 MORC proteins influence TF binding through chromatin compaction. **a** Violin plot showing expression levels of genes proximal to MORC7A with Col-0, *morchex* mutant, Ler (wild type background for *lug* mutant), and *lug* mutant. P values were estimated by the two-sided Wilcoxon rank-sum test. **b** Expression levels of transcriptional factors: SEP3, PIF4, ARF6/8, TPR1, LUG, and SEU (TFs with MORC7A peaks in their promoter regions), with Col-0 and *morchex* mutants following heat treatment. **c** Transcriptomic changes of *morchex* mutants under normal conditions. **d** Transcriptomic changes of *morchex* mutants after 30 min of heat treatment. **e** TPL and LUG binding over MORC7A-unique, MORC7B-unique, MORC7-Pol V Common, and Pol V unique regions. **f** A representative screenshot showing increased binding of TPL and LUG on MORC7A-unique regions in the *morchex* mutant. **g** Correlation of TPL/LUG binding and ATAC-seq alterations with MORC7 binding intensity in *morchex* mutant. **h** Boxplot showing the expression levels of genes directly regulated by LUG in Col-0 and *morchex* mutants following heat treatment for 30 min (T30). *P* values were estimated by the two-sided Wilcoxon rank-sum test. **i** A proposed model of the RdDM-independent functions of MORC proteins

Discussion

We previously reported that MORC proteins are localized to sites of RdDM throughout the genome, and function as molecular tethers to facilitate the efficient establishment of RdDM [7]. We showed that this RdDM-related function of MORC proteins is

critical for de novo transgene silencing [7, 23]; however, this model does not explain other functions of MORC proteins. For example, MORC1 and MORC6 were shown to work downstream of DNA methylation to repress the expression of both the endogenous *SDC* gene and an *SDC* transgene, as well as other DNA-methylated targets in the genome [9]. In addition, *morc* mutants display various disease phenotypes; for example, Kang et al. [8] reported that *morc1* is susceptible to Turnip Crinkle Virus (TRV), while Harris et al. [6] reported that *morchex* is susceptible to the *Hyaloperonospora arabidopsidis* (Hpa) strain, Emwa1. However, the molecular mechanisms underlying the additional functions of the MORC proteins remain unknown.

Here, we investigated the function of MORC7 in regions where RdDM does not occur, particularly those near genes where no DNA methylation is present. We found that MORC proteins reduce chromatin accessibility within these regions. Previous in vitro studies showed that *C. elegans* MORC1 homodimers can topologically entrap and condense DNA through further oligomerization of MORC1 proteins [2]. In addition, Arabidopsis *morc* mutants display pericentromeric heterochromatin decondensation [9], which takes place with minimal losses of DNA methylation throughout the genome. This indicates that MORC proteins contribute to chromatin compaction independently of DNA methylation [9]. We show here that MORC proteins reduce chromatin accessibility in methylation-free promoter regions of DNA, which may explain their mechanism for methylation-independent gene regulation. We suggest that Arabidopsis MORCs may use a similar mechanism of chromatin compaction to that of *C. elegans* MORC1 — compacting chromatin by topological entrapment, thereby reducing its accessibility to TFs.

Plant MORCs have been implicated in plant pathogen responses. MORCs promote resistance in some plant species and inhibit defense responses in others [8]. Upregulation of protein-coding genes was previously shown in *morc4 morc7*; although, the underlying mechanism of this was unknown [6]. Here, we report that MORC proteins regulate gene expression by compacting chromatin in promoter regions, thereby preventing access by TFs. In addition, MORCs preferentially bound to the promoter regions of TF genes, contributing to their regulation, and our crosslinked IP-MS data suggested that MORCs are in close proximity to many TFs. A previous study suggested that the proteins SUVH2 and SUVH9 bind to methylated DNA and recruit MORC proteins to RdDM loci to facilitate the efficiency of RdDM and gene silencing [25]. However, the question of how MORC proteins are recruited to regions devoid of RdDM remains to be answered. Interestingly, we observed that many of TFs interacting with MORC7 bind to their own promoters suggesting regulation by a feed-forward loop, which may amplify the effects of MORCs on transcriptional networks.

Finally, we showed that MORC proteins are important for the regulation of gene expression, particularly under stress conditions. We also found altered expression of heat-responsive genes in *morchex*. Like with its role in plant pathogen defense response, it seems likely that the role of MORCs in stress responses relates to its effects on chromatin compaction of promoter regions and TF networks.

Conclusions

MORC proteins have a broad binding spectrum in the genome and appear to participate in at least three separate processes. They co-localize to sites of RdDM, facilitating efficient DNA methylation establishment [7], they are needed to repress DNA methylated

areas of pericentromeric heterochromatin in a DNA methylation-independent manner [9], and they co-localize with TFs in unmethylated promoter regions, regulating TF binding and gene expression by altering chromatin accessibility (Fig. 5i). Although it seems likely that MORC act in each of these processes by topologically entrapping DNA, there are likely mechanistic differences that can explain the localization and function of MORCs in these three different epigenetic environments in the genome.

Methods

Plant materials and growth conditions

All plants in this study were grown in standard greenhouse conditions (22–25 °C, 16 h light/8 h dark). The following plant materials were used in this study: *morchex* consisting of *morc1-2* (SAIL_893_B06), *morc2-1* (SALK_072774C), *morc4-1* (SALK_051729), *morc5-1* (SALK_049050C), *morc6-3* (GABI_599B06), and *morc7-1* (SALK_051729). For heat treatments, plants were grown under 37 °C for 0.5 h and put back to normal temperature for 48 h for recovery.

Epitope-tagged transgenic lines

Full-length genomic DNA fragments, including native promoter sequences, were cloned into pENTR/D vectors (Invitrogen), and then into modified destination vectors carrying 3xFLAG with LR Clonase (Invitrogen). All primers used in this study are available in Additional file 5: Table S4.

Nuclei extraction and ATAC-seq library preparation

The nuclei collection process from inflorescence and meristem tissues was performed in accordance with previously described methods [26, 27]. Freshly isolated nuclei were used for ATAC-seq, as described elsewhere [28]. Inflorescence tissues were collected for extraction of nuclei as follows: 5 g (approximately) of inflorescence tissue was collected and immediately transferred into the ice-cold grinding buffer (300 mM sucrose, 20 mM Tris pH 8, 5 mM $MgCl_2$, 5 mM KCl, 0.2% Triton X-100, 5 mM β-mercaptoethanol, and 35% glycerol); the samples were then ground with Omni International General Laboratory Homogenizer at 4 °C, and filtered through a two-layer Miracloth using a 40-μm nylon mesh Cell Strainer (Fisher). Samples were spin filtered for 10 min at 3000 g, the supernatant was discarded, and the pellet was resuspended with 25 ml of grinding buffer using a Dounce homogenizer. The wash step was performed twice in total. Nuclei were then resuspended in 0.5 ml of freezing buffer (50 mM Tris pH 8, 5 mM $MgCl_2$, 20% glycerol, and 5 mM β-mercaptoethanol). Nuclei were then subjected to a transposition reaction with Tn5 (Illumina). For the transposition reaction, 25 μl of 2 × DMF (66 mM Tris–acetate pH 7.8, 132 mM K-Acetate, 20 mM Mg-Acetate, and 32% DMF) was mixed with 2.5 μl Tn5 and 22.5 μl nuclei suspension at 37 °C for 30 min. The transposed DNA fragments were then purified with ChIP DNA Clean & Concentrator Kit (Zymo). Libraries were prepared with Phusion High-Fidelity DNA Polymerase (NEB), in a system containing: 12.5 μl 2 × Phusion, 1.25 μl 10 mM Ad1 primer, 1.25 μl 10 mM Ad2 primer, 4 μl ddH2O, and 6 μl purified

transposed DNA fragments. The ATAC-seq libraries were sequenced on a NovaSeq 6000 sequencer (Illumina).

RNA-seq library preparation

Total RNAs were extracted from ~ 100 mg of flower buds using TRIzol and the Direct-zol RNA Miniprep kit (Zymo, R2050). Sequencing libraries were prepared using the TruSeq Stranded mRNA Library Prep kit (Illumina), according to the manufacturer's instructions, and sequenced on a NovaSeq 6000 sequencer (Illumina).

ChIP-seq library preparation

10 g of inflorescence and meristem tissues were used for ChIP-seq. ChIP assays were performed as has been described previously [29]. Briefly, 2–4 g of flower tissue was collected from 4- to 5-week-old plants, and ground with liquid nitrogen. 1% formaldehyde containing a nuclei isolation buffer was used to fix the chromatin for ten minutes. Freshly prepared glycine was then used to terminate the crossing reaction. Shearing was performed via Bioruptor Plus (Diagenode), and immunoprecipitations with antibodies were performed overnight at 4 °C. The anti-FLAG M2 (Sigma) antibody was used in this study. Magnetic Protein A and Protein G Dynabeads (Invitrogen) were added and incubated at 4 °C for 2 h. The reverse crosslink was performed overnight at 65 °C. The protein-DNA mix was then treated with Protease K (Invitrogen) at 45 °C for 4 h. The DNA was purified and precipitated with 3 M Sodium Acetate (Invitrogen), glycoBlue (Invitrogen), and ethanol overnight at − 20 °C. The precipitated DNA was then used for library preparation using the Ovation Ultra Low System V2 kit (NuGEN), which was then sequenced using an Illumina NovaSeq 6000 sequencer.

Small RNA-seq analysis

Small RNA-seq reads were downloaded from a previous paper [30]. Adaptor sequence (TGGAATTCTCGG) was trimmed with trim_galore, and trimmed reads were mapped to the reference genome TAIR10 using Bowtie2 with only one unique hit and zero mismatches [31].

ATAC-seq analysis

ATAC-seq read adaptors were removed using trim_galore. The reads were then mapped to the Arabidopsis thaliana reference genome, TAIR10, using Bowtie2 (-X 2000 -m 1) [31]. Reads of chloroplast and mitochondrial DNA were filtered out and duplicate reads were removed using Samtools [32]. ATAC-Seq open chromatin peaks of each replicate were called using MACS2 with parameters of -p 0.01 –nomodel –shift -100 –extsize 200. Consensus sets of chromatin peaks for all samples were merged by bedtools (v2.26.0) intersect allowing a distance of 10 base pairs [33]. Following this, edgeR was used to define significant changes between peaks [fold change, (FC) > 2 and false discovery rate, (FDR) < 0.05] [34]. ATAC-seq peak distributions were annotated using ChIPseeker [35]. TF footprints were analyzed by TOBIAS [21] with 572 plant TF motifs downloaded from JASPAR (http://jaspar.genereg.net/) [22].

RNA-seq analysis

Cleaned short reads were aligned to the reference genome, TAIR10, by Bowtie2 (v2.1.0) [31]. Expression abundance was then calculated by RSEM using the default parameters [36]. Heatmaps were visualized using the R package pheatmap. Differential expression analysis was conducted using edgeR [34]. A threshold of p-value < 0.05 and fold change > 2 were used to decide whether there were any significant differences in expression between samples.

ChIP-seq analysis

ChIP-seq data was aligned to the TAIR10 reference genome with Bowtie2 (v2.1.0) [31], only including uniquely mapped reads without any mismatches. Duplicated reads were removed by Samtools. ChIP-seq peaks were called by MACS2 (v2.1.1) and annotated using ChIPseeker [35]. Differential peaks were called by the bdgdiff function in MACS2 [37]. ChIP-seq data metaplots were plotted by deeptools (v2.5.1) [38]. Correlation of MORC7 with ChIP-seq data was conducted with ChromHMM [39]. H3K9ac, H3K27ac, H4K16ac, H3K4me1, H3K4me3, H3K36me2, H3K36me3, H3K9me2, H3K27me3, Pol II, and Pol V, as published previously, were included in this analysis (Additional file 6: Table S5). Motif enrichment analysis was performed with MEME (v5.0.5) [40].

Whole-genome bisulfite sequencing (BS-seq) analysis

Previously published whole-genome bisulfite sequencing data for *morc* mutants and wild type was reanalyzed [6]. Briefly, Trim_galore (http://www.bioinformatics.babraham.ac.uk/projects/trim_galore/) was used to trim adapters. BS-seq reads were aligned to the TAIR10 reference genome by BSMAP (v2.90), allowing two mismatches and one best hit (-v 2 -w 1) [41]. Reads with three or more consecutive CHH sites were considered to be unconverted reads and were filtered out. DNA methylation levels were defined as #C/ (#C + #T).

Supplementary Information

The online version contains supplementary material available at https://doi.org/10.1186/s13059-023-02939-4.

Additional file 1: Figure S1. Chromatin states of MORC7. **Figure S2.** Small RNA data over MORC7 peaks. **Figure S3.** Examples showing MORC7 enrichment over the promoter regions of the *TOPLESS* genes. **Figure S4.** MORC7 associates with some TFs. **Figure S5.** Metaplot and heatmap showing chromatin accessibility changes. **Figure S6.** Volcano plot showing TF changes for ZF off-target sites. **Figure S7.** Expression levels of genes in the primary shoot apical meristem specification pathway, with and without heat treatment, in Col-0 and *morchex* mutants. **Figure S8.** Motif enrichment of TPL and LUG peaks identified in Col-0 or *morchex* mutant. **Figure S9.** Metaplot and heatmap showing ChIP-seq signals over peaks detected in *morchex* mutant.

Additional file 2: Table S1. Genes proximal to MORC7A-unique, MORC7B-unique, MORC7-Pol V Common, and Pol V-unique peaks.

Additional file 3: Table S2. List of MORC7 interacting proteins.

Additional file 4: Table S3. Expression level of LUG directly regulated genes in Ler and lug mutant.

Additional file 5: Table S4. Primers used in this study.

Additional file 6: Table S5. Published ChIP-seq data used for ChromHMM states analysis.

Additional file 7. Review history.

Acknowledgements

We thank members of Jacobsen laboratory for the helpful discussion. We are grateful to M. Akhavan and the UCLA BSCRC High Throughput BioSequencing Core for their technical assistance. We also thank Life Science Editors (https://www.lifescienceeditors.com/) for editing assistance.

Peer review information
Wenjing She was the primary editor of this article and managed its editorial process and peer review in collaboration with the rest of the editorial team.

Review history
The review history is available as Additional file 7.

Authors' contributions
ZZ, YX, and SEJ conceived the study. ZZ, YX, and CJH performed experiments assisted by MW, ZL, YK, ML, and JZ. SF performed high throughput sequencing. YJA and JAW performed IP-MS. ZZ, YX, and SEJ wrote the manuscript with help from all authors. All authors approved the final version of the manuscript and agree on the content and conclusions.

Funding
The work in the Jacobsen laboratory was supported by NIH grant R35 GM130272 and a grant from the W.M. Keck Foundation. Steven E. Jacobsen is an investigator of the Howard Hughes Medical Institute.

Availability of data and materials
Data supporting the findings of this work are available within the paper and its Supplementary Information files. All high-throughput sequencing data generated in this study are accessible at NCBI's Gene Expression Omnibus (GEO) via GEO Series accession number GSE212801 [42]. The customized codes used in this study are available Github [43], Figshare [44], and is released under the terms of the GNU General Public License (GPL) version 3.0 (https://opensource.org/license/gpl-3-0/). ChIP-seq data from the following studies and accession numbers were used: Liu et al. [26] (GSM2667837 [45]), Liu et al. [46] (GSM4275144 [47], GSM4275146 [48]), Zhu et al. [49] (SRR1509479 [50]), Harris et al. [51] (GSM2897853 [52]), Jégu et al. [53] (GSM2366606 [54]), Chen et al. [55] (GSM2882803 [56]), Lu et al. [57] (GSM3674621 [58]), and Zhong et al. [59] (GSM5684049 [60], GSM5684053 [61], GSM5684057 [62]).

Declarations

Ethics approval and consent to participate
Not applicable.

Consent for publication
Not applicable.

Competing interests
The authors declare that they have no competing interests.

Received: 4 November 2022 Accepted: 17 April 2023
Published online: 26 April 2023

References

1. Dong W, Vannozzi A, Chen F, Hu Y, Chen Z, Zhang L. MORC domain definition and evolutionary analysis of the MORC gene family in green plants. Genome Biol Evol. 2018;10:1730–44.
2. Kim H, Yen L, Wongpalee SP, Kirshner JA, Mehta N, Xue Y, et al. The Gene-Silencing Protein MORC-1 Topologically Entraps DNA and Forms Multimeric Assemblies to Cause DNA Compaction. Mol Cell. 2019;75:700-710.e6.
3. Tchasovnikarova IA, Timms RT, Douse CH, Roberts RC, Dougan G, Kingston RE, et al. Hyperactivation of HUSH complex function by Charcot-Marie-Tooth disease mutation in MORC2. Nat Genet. 2017;49:1035–44.
4. Pastor WA, Stroud H, Nee K, Liu W, Pezic D, Manakov S, et al. MORC1 represses transposable elements in the mouse male germline. Nat Commun. 2014;5:5795.
5. Desai VP, Chouaref J, Wu H, Pastor WA, Kan RL, Oey HM, et al. The role of MORC3 in silencing transposable elements in mouse embryonic stem cells. Epigenetics Chromatin. 2021;14:1–14.
6. Harris CJ, Husmann D, Liu W, el Kasmi F, Wang H, Papikian A, et al. Arabidopsis AtMORC4 and AtMORC7 Form Nuclear Bodies and Repress a Large Number of Protein-Coding Genes. PLoS Genet. 2016;12:e1005998–e1005998.
7. Xue Y, Zhong Z, Harris CJ, Gallego-Bartolomé J, Wang M, Picard C, et al. Arabidopsis MORC proteins function in the efficient establishment of RNA directed DNA methylation. Nat Commun. 2021;12:4292.
8. Kang H-G, Kuhl JC, Kachroo P, Klessig DF. CRT1, an Arabidopsis ATPase that Interacts with Diverse Resistance Proteins and Modulates Disease Resistance to Turnip Crinkle Virus. Cell Host Microbe. 2008;3:48–57.
9. Moissiard G, Cokus SJ, Cary J, Feng S, Billi AC, Stroud H, et al. MORC family ATPases required for heterochromatin condensation and gene silencing. Science. 2012;336:1448–51.
10. Chen G, Courey AJ. Groucho/TLE family proteins and transcriptional repression. Gene. 2000;249:1–16.
11. Papamichos-Chronakis M, Petrakis T, Ktistaki E, Topalidou I, Tzamarias D. Cti6, a PHD Domain Protein, Bridges the Cyc8-Tup1 Corepressor and the SAGA Coactivator to Overcome Repression at GAL1. Mol Cell. 2002;9:1297–305.
12. Proft M, Struhl K. Hog1 Kinase Converts the Sko1-Cyc8-Tup1 Repressor Complex into an Activator that Recruits SAGA and SWI/SNF in Response to Osmotic Stress. Mol Cell. 2002;9:1307–17.
13. Li S, Yen L, Pastor WA, Johnston JB, Du J, Shew CJ, et al. Mouse MORC3 is a GHKL ATPase that localizes to H3K4me3 marked chromatin. Proc Natl Acad Sci U S A. 2016;113:E5108–16.
14. Sequeira-Mendes J, Aragüez I, Peiró R, Mendez-Giraldez R, Zhang X, Jacobsen SE, et al. The functional topography of the Arabidopsis genome is organized in a reduced number of linear motifs of chromatin states. Plant Cell. 2014;26:2351–66.

15. de Clercq I, van de Velde J, Luo X, Liu L, Storme V, van Bel M, et al. Integrative inference of transcriptional networks in Arabidopsis yields novel ROS signalling regulators. Nat Plants. 2021;7:500–13.
16. Ashburner M, Ball CA, Blake JA, Botstein D, Butler H, Cherry JM, et al. Gene Ontology: tool for the unification of biology. Nat Genet. 2000;25:25.
17. O'Malley RC, Huang SSC, Song L, Lewsey MG, Bartlett A, Nery JR, et al. Cistrome and Epicistrome Features Shape the Regulatory DNA Landscape. Cell. 2016;165:1280–92.
18. Oh E, Zhu J-Y, Wang Z-Y. Interaction between BZR1 and PIF4 integrates brassinosteroid and environmental responses. Nat Cell Biol. 2012;14:802–9.
19. Oh E, Zhu J-Y, Bai M-Y, Arenhart RA, Sun Y, Wang Z-Y. Cell elongation is regulated through a central circuit of interacting transcription factors in the Arabidopsis hypocotyl. Elife. 2014;3: e03031.
20. Griebel T, Lapin D, Locci F, Kracher B, Bautor J, Qiu J, et al. Topless-related 1 mitigates physiological damage and growth penalties of induced immunity. BioRxiv. 2021;2021.07.07.451397. Available from: https://doi.org/10.1101/2021.07.07.451397. Cited 2022 Nov 15.
21. Bentsen M, Goymann P, Schultheis H, Klee K, Petrova A, Wiegandt R, et al. ATAC-seq footprinting unravels kinetics of transcription factor binding during zygotic genome activation. Nat Commun. 2020;11:4267.
22. Khan A, Fornes O, Stigliani A, Gheorghe M, Castro-Mondragon JA, van der Lee R, et al. JASPAR 2018: update of the open-access database of transcription factor binding profiles and its web framework. Nucleic Acids Res. 2018;46:D260–6.
23. Gallego-Bartolome J, Liu W, Kuo PH, Feng S, Ghoshal B, Gardiner J, et al. Co-targeting RNA polymerases IV and V promotes efficient de novo DNA methylation in Arabidopsis. Cell. 2019;176(1068–1082): e19.
24. Kumar SV, Lucyshyn D, Jaeger KE, Alós E, Alvey E, Harberd NP, et al. Transcription factor PIF4 controls the thermosensory activation of flowering. Nature. 2012;484:242–5.
25. Liu Z-W, Shao C-R, Zhang C-J, Zhou J-X, Zhang S-W, Li L, et al. The SET domain proteins SUVH2 and SUVH9 are required for Pol V occupancy at RNA-directed DNA methylation loci. PLoS Genet. 2014;10: e1003948.
26. Liu W, Duttke SH, Hetzel J, Groth M, Feng S, Gallego-Bartolome J, et al. RNA-directed DNA methylation involves co-transcriptional small-RNA-guided slicing of polymerase v transcripts in Arabidopsis. Nat Plants. 2018;4:181–8.
27. Zhong Z, Feng S, Duttke SH, Potok ME, Zhang Y, Gallego-Bartolomé J, et al. DNA methylation-linked chromatin accessibility affects genomic architecture in Arabidopsis. Proc Natl Acad Sci U S A. 2021;118:e2023347118.
28. Buenrostro JD, Giresi PG, Zaba LC, Chang HY, Greenleaf WJ. Transposition of native chromatin for fast and sensitive epigenomic profiling of open chromatin, DNA-binding proteins and nucleosome position. Nat Methods. 2013;10:1213–8.
29. Zhong X, Hale CJ, Law JA, Johnson LM, Feng S, Tu A, et al. DDR complex facilitates global association of RNA polymerase V to promoters and evolutionarily young transposons. Nat Struct Mol Biol. 2012;19:870–5.
30. Zhai J, Bischof S, Wang H, Feng S, Lee T, Teng C, et al. A one precursor one siRNA model for Pol IV-dependent siRNA biogenesis. Cell. 2015;163:445–55.
31. Langmead B, Salzberg SL. Fast gapped-read alignment with Bowtie 2. Nat Methods. 2012;9:357–9.
32. Li H, Handsaker B, Wysoker A, Fennell T, Ruan J, Homer N, et al. The sequence alignment/map format and SAMtools. Bioinformatics. 2009;25:2078–9.
33. Quinlan AR, Hall IM. BEDTools: a flexible suite of utilities for comparing genomic features. Bioinformatics. 2010;26:841–2.
34. Robinson MD, McCarthy DJ, Smyth GK. edgeR: a Bioconductor package for differential expression analysis of digital gene expression data. Bioinformatics. 2010;26:139–40.
35. Yu G, Wang L-G, He Q-Y. ChIPseeker: an R/Bioconductor package for ChIP peak annotation, comparison and visualization. Bioinformatics. 2015;31:2382–3.
36. Li B, Dewey CN. RSEM: accurate transcript quantification from RNA-Seq data with or without a reference genome. BMC Bioinformatics. 2011;12:1–16.
37. Zhang Y, Liu T, Meyer CA, Eeckhoute J, Johnson DS, Bernstein BE, et al. Model-based Analysis of ChIP-Seq (MACS). Genome Biol. 2008;9:R137.
38. Ramírez F, Dündar F, Diehl S, Grüning BA, Manke T. deepTools: a flexible platform for exploring deep-sequencing data. Nucleic Acids Res. 2014;42:W187–91.
39. Ernst J, Kellis M. Chromatin-state discovery and genome annotation with ChromHMM. Nat Protoc. 2017;12:2478–92.
40. Bailey TL, Boden M, Buske FA, Frith M, Grant CE, Clementi L, et al. MEME SUITE: tools for motif discovery and searching. Nucleic Acids Res. 2009;37:W202–8.
41. Xi Y, Li W. BSMAP: whole genome bisulfite sequence MAPping program. BMC Bioinformatics. 2009;10:232.
42. Zhong Z, Xue Y. MORC proteins regulate transcription factor binding by mediating chromatin compaction in active chromatin regions. GSE212801. Gene Expression Omnibus. 2023. https://www.ncbi.nlm.nih.gov/geo/query/acc.cgi?acc=GSE212801. Accessed June 2021.
43. Zhong Z. MORC proteins regulate transcription factor binding by mediating chromatin compaction in active chromatin regions. Github. 2023. https://github.com/Zhenhuiz/MORC_TF_project. Accessed Mar 2023.
44. Zhong Z. MORC proteins regulate transcription factor binding by mediating chromatin compaction in active chromatin regions. Figshare. 2023. https://doi.org/10.6084/m9.figshare.22647559. Accessed Mar 2023.
45. Liu W. Pol V ChIP-seq data. GSM2667837. Gene Expression Omnibus. 2018. https://www.ncbi.nlm.nih.gov/geo/query/acc.cgi?acc=GSM2667837. Accessed June 2021.
46. Liu Q, Bischof S, Harris CJ, Zhong Z, Zhan L, Nguyen C, et al. The characterization of Mediator 12 and 13 as conditional positive gene regulators in Arabidopsis. Nat Commun. 2020;11:1–13.
47. Liu Q. H3K4me3 ChIP-seq data. GSM4275144. Gene Expression Omnibus. 2020. https://www.ncbi.nlm.nih.gov/geo/query/acc.cgi?acc=GSM4275144. Accessed June 2021.
48. Liu Q. H3K27me3 ChIP-seq data. GSM4275146. Gene Expression Omnibus. 2020. https://www.ncbi.nlm.nih.gov/geo/query/acc.cgi?acc=GSM4275146. Accessed June 2021.
49. Zhu B, Zhang W, Zhang T, Liu B, Jiang J. Genome-wide prediction and validation of intergenic enhancers in Arabidopsis using open chromatin signatures. Plant Cell. 2015;27:2415–26.

50. Zhu B. H3K27ac ChIP-seq data. GSM4275146. Sequence Read Archive. 2015. https://trace.ncbi.nlm.nih.gov/Traces/?view=run_browser&acc=SRR1509479. Accessed June 2021.
51. Jake Harris C, Scheibe M, Pop Wongpalee S, Liu W, Cornett EM, Vaughan RM, et al. A DNA methylation reader complex that enhances gene transcription. Science. 2018;6419:1182–6.
52. Jake Harris C. H3K9me2 ChIP-seq data. GSM2897853. Gene Expression Omnibus. 2018. https://www.ncbi.nlm.nih.gov/geo/query/acc.cgi?acc=GSM2897853. Accessed June 2021.
53. Jégu T, Veluchamy A, Ramirez-Prado JS, Rizzi-Paillet C, Perez M, Lhomme A, et al. The Arabidopsis SWI/SNF protein BAF60 mediates seedling growth control by modulating DNA accessibility. Genome Biol. 2017;18:114.
54. Jégu T. H3K9ac ChIP-seq data. GSM2366606. Gene Expression Omnibus. 2017. https://www.ncbi.nlm.nih.gov/geo/query/acc.cgi?acc=GSM2366606. Accessed June 2021.
55. Chen X, Lu L, Qian S, Scalf M, Smith LM, Zhong X. Canonical and noncanonical actions of Arabidopsis histone deacetylases in ribosomal RNA processing. Plant Cell. 2018;30:134–52.
56. Chen X. H4K16ac ChIP-seq data. GSM2882803. Gene Expression Omnibus. 2018. https://www.ncbi.nlm.nih.gov/geo/query/acc.cgi?acc=GSM2882803. Accessed June 2021.
57. Lu Z, Marand AP, Ricci WA, Ethridge CL, Zhang X, Schmitz RJ. The prevalence, evolution and chromatin signatures of plant regulatory elements. Nat Plants. 2019;5:1250–9.
58. Lu Z. H3K4me1 ChIP-seq data. GSM3674621. Gene Expression Omnibus. 2019. https://www.ncbi.nlm.nih.gov/geo/query/acc.cgi?acc=GSM3674621. Accessed June 2021.
59. Zhong Z, Wang Y, Wang M, Yang F, Thomas QA, Xue Y, Zhang Y, et al. Histone chaperone ASF1 mediates H3. 3-H4 deposition in Arabidopsis. Nat Commun. 2022;13:6970.
60. Zhong Z. H3K36me2 ChIP-seq data. GSM5684049. Gene Expression Omnibus. 2022. https://www.ncbi.nlm.nih.gov/geo/query/acc.cgi?acc=GSM5684049. Accessed June 2022.
61. Zhong Z. H3K36me3 ChIP-seq data. GSM5684053. Gene Expression Omnibus. 2022. https://www.ncbi.nlm.nih.gov/geo/query/acc.cgi?acc=GSM5684053. Accessed June 2022.
62. Zhong Z. Pol II ChIP-seq data. GSM5684057. Gene Expression Omnibus. 2022. https://www.ncbi.nlm.nih.gov/geo/query/acc.cgi?acc=GSM5684057. Accessed June 2022.

Publisher's Note